6-1990

Full Modeling of Field-Assisted Ion Exchange for Graded Index Buried Channel Optical Waveguides

Jacques Albert
Wilfrid Laurier University

John W.Y. Lit
Wilfrid Laurier University, jlit@wlu.ca

Full modeling of field-assisted ion exchange for graded index buried channel optical waveguides

Jacques Albert and John W. Y. Lit

The numerical modeling of field-assisted ion exchange in glass through a finite aperture is carried out. The effects of unequal ion mobilities and thermal diffusion are included we believe for the first time in the 2-D case. This allows for the modeling of optical channel waveguides with graded index profiles. It is demonstrated that annealing of backdiffused channel guides is far superior to backdiffusion alone in improving their circular symmetry for better coupling to optical fibers.

I. Introduction

Making passive integrated optical devices depends greatly on our ability to control their properties by adjusting the fabrication parameters. In the case of ion exchange in glass, the nonlinear diffusion equations governing the exchange of the host ion by the doping ion have been solved numerically in a few important cases. Purely thermal diffusion in both one and two dimensions has been treated successfully as well as field-assisted ion exchange in one dimension (see Ref. 1 for a review). In the 2-D case, however, the proposed solutions are limited to the situation where thermal diffusion can be neglected with respect to the field driven diffusion and where ionic mobilities are equal.[2,3] Proceeding in this manner, it is not possible to model graded index channel optical waveguides and/or small single-mode guides exchanged with relatively weak driving electric fields. In view of the fact that these latter cases are perhaps the most important for integrated optics applications, we feel that an effort to solve this more complex problem is warranted.

The basic equations to be solved are described below. We point out how our solutions go further than previously published work and present some calculated results. These illustrate the possible control over the refractive index profile by modifying the variables involved in the fabrication process.

The mode mismatch due to different cross-sectional shapes is the major cause of insertion losses when a guide made by ion exchange is coupled to a fiber.[4] We demonstrate how a proper sequence of exchange, backdiffusion, and annealing can lead to almost perfectly circular channel index profiles which decrease such insertion losses.

II. Model Description

There are two types of force that act on the exchanging ions. One is due to the gradient in chemical potential; it leads to a flux $\mathbf{J}_D$ of ions proportional to the gradient of their concentration c. The proportionality constant is called D, the diffusion coefficient:

$$\mathbf{J}_D = -D\nabla c. \tag{1}$$

The second force is due to the presence of an electric field in the glass during the exchange. Even in the absence of an externally applied field, the difference in the mobilities of the two types of exchanging ion leads to local charge imbalances that cause an electric field to build up. The ion flux resulting from the field is given by

$$\mathbf{J}_E = c\mu\mathbf{E}. \tag{2}$$

In this equation the mobility μ is related to the diffusion coefficient D by the Einstein relation:

$$\mu = \frac{eD}{kT}, \tag{3}$$

where e is the electron charge, k is Boltzmann's constant, and T is the temperature in kelvins. It has been shown that this relation holds quite well for ionic diffusion in glasses.[5] In ion exchange, two kinds of ion are in motion: the indiffusing ions labeled with subscript a, and the outdiffusing ions labeled b. The two fluxes may be written

$$\mathbf{J}_a = -D_a\left(\nabla c_a - \frac{e\mathbf{E}}{kT}c_a\right), \tag{4}$$

When this work was done both authors were with Wilfrid Laurier University, Department of Physics & Computing, Waterloo, Ontario N2L 3C5, Canada; J. Albert is now with Communications Research Centre, P.O. Box 11490, Station H, Ottawa, Ontario K2H 8S2, Canada.

Received 14 March 1989.
0003-6935/90/182798-07$02.00/0.

$$\mathbf{J}_b = -D_b\left(\nabla c_b - \frac{e\mathbf{E}}{kT} c_b\right). \tag{5}$$

The goal of this calculation is to determine the concentration of the new ions in the glass (c_a) as a function of the fabrication parameters. (The index change induced in the glass is proportional to c_a.[6]) For this, we use the continuity equation:

$$\frac{\partial c_a}{\partial t} = -\nabla \cdot \mathbf{J}_a \tag{6}$$

$$= D_a\left[\nabla^2 c_a - \frac{e}{kT}(c_a \nabla \cdot \mathbf{E} + \mathbf{E} \cdot \nabla c_a)\right]. \tag{7}$$

It is possible to eliminate the term involving the divergence of the electric field by using the following conditions for the electroneutrality of the glass. First, the total ion concentration must be a constant, equal to the initial concentration of host ions.

$$c_a + c_b = c_b(t = 0) = c_0, \tag{8}$$

and (except at the boundaries where the ion sources are located) the divergence of the total flux must be zero:

$$\nabla \cdot (\mathbf{J}_a + \mathbf{J}_b) = 0. \tag{9}$$

From Eq. (8) we get

$$\nabla^2 c_a = -\nabla^2 c_b, \tag{10}$$

and from Eq. (9), with Eqs. (4), (5), and (10),

$$(D_b - D_a)\nabla^2 c_a - (D_b - D_a)\frac{e}{kT}\nabla \cdot (\mathbf{E}c_a) + D_b \frac{e}{kT}\nabla \cdot (\mathbf{E}c_0) = 0. \tag{11}$$

Dividing through by c_0 and isolating the divergence term, we obtain

$$\nabla \cdot \mathbf{E} = \alpha \frac{\mathbf{E} \cdot \nabla c - \dfrac{kT}{e}\nabla^2 c}{1 - \alpha c}, \tag{12}$$

with

$$c = \frac{c_a}{c_0}; \quad \alpha = 1 - \frac{D_a}{D_b}, \tag{13}$$

where c is the normalized concentration of new ions in the glass, and α is a measure of the difference in ion mobilities. Substituting Eq. (12) into Eq. (7) leads to

$$\frac{\partial c}{\partial t} = \frac{D_a}{1 - \alpha c}\left(\nabla^2 c - \frac{e}{kT}\mathbf{E} \cdot \nabla c\right). \tag{14}$$

But we still do not know the value of the local electric field E. In Ref. 2, the imposed electric field was directly substituted into Eq. (14) to solve for c (along with approximations that $\alpha = 0$ and that the first term on the right-hand side was negligible relative to the last one). When α is not equal to zero this is an incorrect procedure since this equation does not reduce to the accepted expression for the nonfield-assisted case (external $E = 0$) (Ref. 7):

$$\frac{\partial c}{\partial t} = D_a \nabla \cdot \left(\frac{1}{1 - \alpha c}\nabla c\right) \tag{15}$$

$$= \frac{D_a}{1 - \alpha c}\left[\nabla^2 c + \frac{\alpha(\nabla c)^2}{1 - \alpha c}\right]. \tag{16}$$

The correct procedure is indicated in Ref. 8 for the case and extended here to the 1-D situation. It involves expressing $\mathbf{E}$ in terms of the total flux of ions in the glass $\mathbf{J}_0$. This is found by adding Eqs. (4) and (5).

$$\frac{\mathbf{J}_0}{c_0 D_b} = \frac{e\mathbf{E}}{kT}\left[\frac{D_a c}{D_b} + (1 - c)\right] + \left(1 - \frac{D_a}{D_b}\right)\nabla c. \tag{17}$$

This leads to

$$\frac{e\mathbf{E}}{kT} = \frac{\dfrac{\mathbf{J}_0}{c_0 D_b} - \alpha \nabla c}{1 - \alpha c}. \tag{18}$$

We can write

$$\mathbf{E} = \mathbf{E}_{\text{ext}} + \mathbf{E}_{\text{diff}}, \tag{19}$$

where

$$\frac{e\mathbf{E}_{\text{ext}}}{kT} = \frac{\mathbf{J}_0}{c_0 D_b(1 - \alpha c)}, \tag{20}$$

$$\frac{e\mathbf{E}_{\text{diff}}}{kT} = \frac{-\alpha \nabla c}{(1 - \alpha c)}. \tag{21}$$

This result shows that when there is no externally applied field (and, therefore, a zero net flux $\mathbf{J}_0$), an electric field is still present, which is due to the unequal ion mobilities ($\alpha \neq 0$). Substituting Eqs. (18)–(21) into Eq. (12) yields the correct expression for the change of concentration:

$$\frac{\partial c}{\partial t} = \frac{D_a}{1 - \alpha c}\left[\nabla^2 c + \frac{\alpha(\nabla c)^2}{1 - \alpha c} - \frac{e\mathbf{E}_{\text{ext}}}{kT}\nabla c\right]. \tag{22}$$

It is now obvious that Eq. (22) reduces correctly to Eq. (16) when the external field is zero. Note that when the field is expressed as in Eq. (18), the discrepancy noted in Ref. 9 between the expressions derived in Refs. 2 and 8 is removed.

Equation (22) appears in Ref. 8 in 1-D form [using the correspondence between J_0 and E_{ext} given by Eq. (20)]. Therefore, its derivation in the 2-D context presented no difficulty. The significant difference in this case is that the net current density J_0 is now a vector quantity and cannot be obtained readily from the experimental parameters. [In the planar case it is given by $I/(FA)$, where I is the total current, F is Faraday's constant, and A is the area of the surface of the substrate through which the current flows.[8]] In Ref. 2, where 2-D results are obtained, the derivation of the equations stopped at our Eq. (14), and an approximate expression for the total field $\mathbf{E}$ (considered there to be equal to the external field) was used. By proceeding further in the derivation we are able to limit the approximation to the external contribution to the total field. The other advantage in using Eq. (22) in the 2-D case is that the thermal diffusion and unequal mobility contributions are explicitly kept (first

and second terms in the parentheses, respectively) and allow graded index structures to be modeled.

We can now proceed with the calculation of $\mathbf{E}_{ext}$ from measurable experimental quantities. In Ref. 2, it is calculated from Laplace's equation along with suitable boundary conditions. This can be justified as follows.

In a steady state situation (unfortunately not always achieved, especially for short exchange times), the curl of the electric field is zero. Therefore, it can be expressed as the gradient of a scalar potential. Furthermore, its divergence would be zero if the conductivity was homogeneous throughout the exchange domain. This steady state homogeneous conductivity field derives from a potential which obeys Laplace's equation and constitutes an approximation for the external field in the glass.

As far as the boundary conditions are concerned, the potential in the openings of the mask at the surface of the substrate is constant, because the ions on the melt side are free to move laterally to cancel any gradient. The situation is analogous to the calculation of the electric field of the TEM mode of a triplate transmission line with electrodes corresponding to the mask openings on either side of the substrate.[2]

The electric field of the triplate line is given by the following formula in terms of the geometry and applied voltage[10]:

$$E_y + iE_x = i\frac{\pi}{2d}\frac{V}{K'(\beta)}\left(\frac{\tanh^2 u - 1}{\tanh^2 u - \beta^2}\right)^{1/2} \tag{23}$$

with

$$u = \frac{\pi(y - ix)}{2d} \text{ and } \beta = \tanh(\pi D/4d), \tag{24}$$

where V is the applied voltage, d is the thickness of the substrate, $K'(\beta)$ is the Jacobian elliptic function, and D is the width of the opening in the mask. The geometrical parameters as well as a typical set of field lines (or net flux) are shown in Fig. 1. Equation (22) is then fully determined in terms of the fabrication parameters and can be solved.

The method used to solve the equation is given in the next section, and results are presented for the particular case of a large multimode channel guide. However, it is possible to generalize the results by using the fact that the partial differential equation is scalable. If all the linear dimensions of the problem (including d and D) are divided by a common factor S, Eq. (22) may be written

$$\frac{\partial c}{\partial \Phi} = \frac{1}{1 - \alpha c}\left[\nabla'^2 c + \frac{\alpha(\nabla' c)^2}{1 - \alpha c} - \frac{e\mathbf{E}'_{ext}}{kT}\nabla' c\right], \tag{25}$$

with

$$\Phi = S^2 D_a t, \quad x' = x/S, \quad y' = y/S, \quad \mathbf{E}'_{ext} = \mathbf{E}_{ext} S \tag{26}$$

(note that E_{ext} is inversely proportional to d).

Therefore, the solution to Eq. (22) or (25) depends only on the variable Φ, and the linear dimensions of any result may be scaled by changing S while keeping the product $S^2 D_a t$ constant! For example, the results

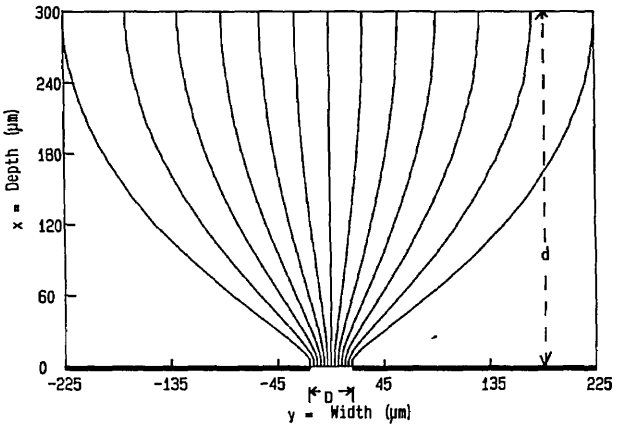

Fig. 1. Geometry of the exchange domain and flux lines of the ionic current. D is the width of the mask opening, and d is the substrate depth.

of the next section become valid in the single-mode regime for $S = 10$ along with $D_a t$ reduced by a factor of 100.

Furthermore, for strong fields, the first two terms on the right-hand side of Eq. (25) become negligible, and the results depend only on the new normalized variable $S^2 D_a t V$. In this strong field limit (this is the regime studied in Ref. 2), the results do not change for a constant value of the product $V^* t$. This is verified in the next section.

III. Numerical Solution

The partial differential equation which describes the field-assisted ion exchange is nonlinear and fairly complex. Its solution must be found numerically, and we have chosen to use a finite-difference explicit method on a discrete grid for the calculation. The time-independent boundary conditions at the top surface are

$$c(0,y) = 1 \quad \left(|y| \le \frac{D}{2}\right), \tag{27}$$

$$\frac{\partial c}{\partial x} = 0 \quad \left(|y| > \frac{D}{2}\right), \tag{28}$$

and all the other boundaries are chosen sufficiently far for the concentration to be fixed at zero throughout the exchange. The grid size is adjusted to each problem by choosing a factor which imposes a sufficient number of grid points in the mask opening.

When the simulation of annealing is performed, the boundary condition at the top surface is changed to one of zero normal gradient [i.e., like Eq. (28) but for all y], which is equivalent to saying that there is no flux normal to the boundary. Finally, for backdiffusion, the surface boundary condition is changed to $c = 0$ (all the surface ions replaced by the ions that were initially in the glass).

To verify the accuracy of the numerical procedures developed for this work, a comparison was made with the 1-D results of Yoshida and Kataoka.[11] The depth profile at the center of an aperture much wider than the final exchange depth should match the 1-D result.

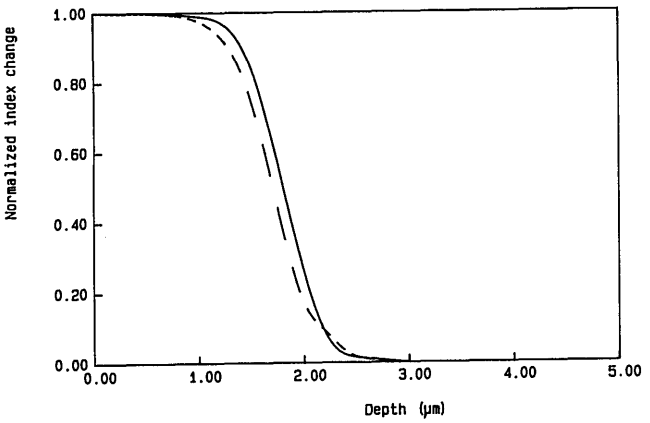

Fig. 2. Comparison between the 1-D result of Ref. 11 (——) and our result (- - -) for $D = 100\ \mu m$, $d = 50\ \mu m$, $T = 616$ K, $D_a = 2.6 \times 10^{-15}\ m^2/s$, $\alpha = 0.9$, $t = 96''$, and $V = 1.6$ V.

This is shown in Fig. 2 for a typical case. The difference is a relatively constant offset of $\sim 0.2\ \mu m$ between the two curves and may be due in part to the fact that it was not practically possible to use as fine a grid for the 2-D calculation because of the prohibitively large number of resulting grid points.

Another verification can be performed by comparing our results with those of Lilienhof *et al.*[2] By using their parameters, our concentration profiles should match their step function profiles but with additional information about the graded transitions between the exchanged and nonexchanged regions of the substrate. Figure 3 shows such a comparison for two cases. They used silver–sodium ion exchange as experimental data to verify their modeling. In this case α is equal to ~ 0.5,[5] and the first case shows how the profile really appears when this information is included in the calculation. Using the same exchange parameters but a slightly different geometry in the second case indicates how dramatically different the profile might become from a step function if α were smaller. These two cases also help to validate our results in the sense that in spite of the more complex calculations which they involve, the size our profiles is the same as theirs but with additional detail in the shape of the transitions.

IV. Single Exchange Results

Because of the shape of the flux lines (see Fig. 1), the guides made with an assisting field suffer from the same predicament as those obtained from a purely thermal process. Their width is approximately equal to the width of the opening in the mask plus twice the exchange depth. This makes it impossible to fabricate guides with unity aspect ratio (depth/width) for good coupling to optical fibers with circular index profiles. This is true regardless of the strength of the driving voltage used. We will see below how the aspect ratio can be improved by using backdiffusion and annealing. A feature of field-assisted guides that is particular to that case is the enhanced exchange depth observed near the edges of a mask larger than the average depth [see Fig. 3(a)]. This is due to an increase in field

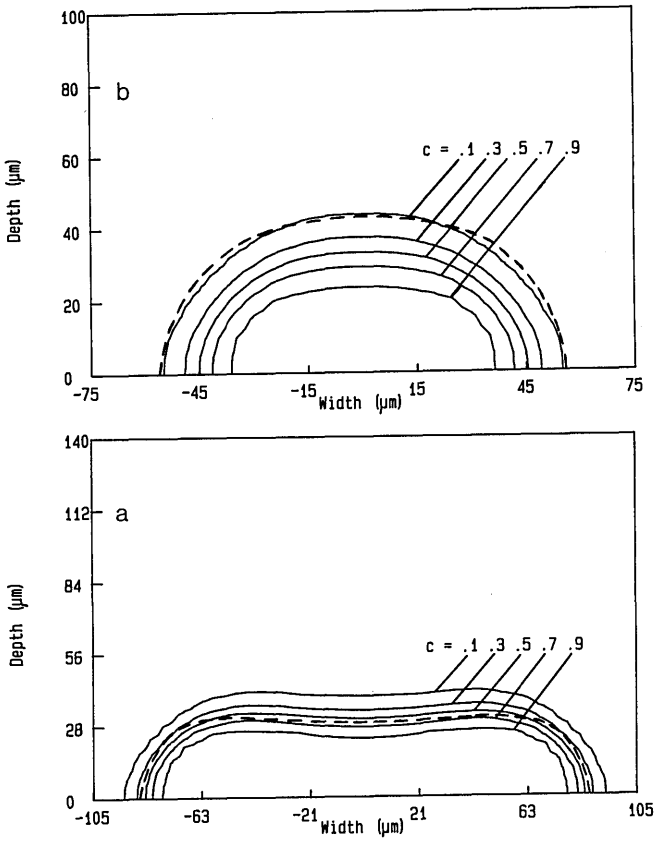

Fig. 3. Comparison between the partial 2-D results of Ref. 2 (dotted contour line marking the boundary of the exchanged area) and our results (set of continuous contour lines): (a) $D = 106\ \mu m$, $d = 300\ \mu m$, $\alpha = 0.5$, $t = 30'$, and $V = 30$ V (other parameters as in Fig. 2); (b) $D = 36\ \mu m$, $\alpha = 0.2$ [others as in (a)].

strength near potential discontinuities (mask opening edges) and has been observed experimentally.[2] A factor which may influence the modeling of this phenomenon (but which is not considered here) is the charge depletion that is believed to occur under the mask area.[12] When the mask aperture is small relative to the exchange depth, the more familiar semicircular pattern is observed [Fig. 3(b)]. Note that in these examples, and those that follow, we always use the exchange parameters given in Ref. 2 to facilitate comparisons between all the cases illustrated.

Among the observations that can be made about 2-D field-assisted ion exchange, many have their equivalent in the 1-D case (see Refs. 8, 9, or 11). The profile moves inside the substrate relatively unchanged as the product $V \times t$ is increased and is independent of the individual values of V and t when their product is constant (Fig. 4). Also, the smoothness of the transition increases with smaller values of α (Figs. 3 and 4). Note that in Ref. 2, abrupt profiles are obtained with $\alpha = 0$, but this is because thermal diffusion is neglected.

The profiles given in our results belong to the regime where the external fields are dominant, as indicated by the appearance of flat constant concentration zones on either side of the transition. However, diffusion terms

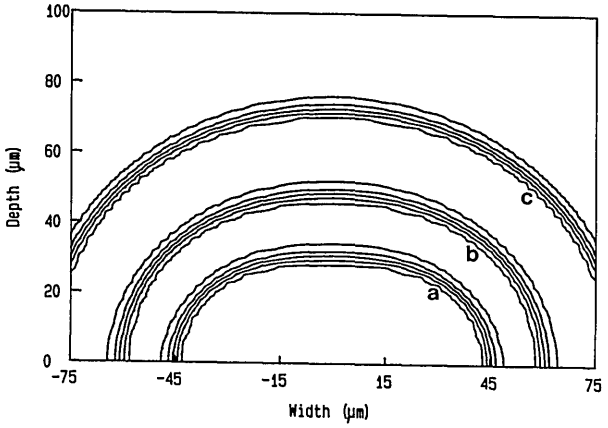

Fig. 4. Evolution of the exchanged profile for $\alpha = 0.7$. In this figure and all the following, the contour lines go from 0.1 to 0.9 as in Fig. 3 with the results normalized to the maximum value: *a*, $D = 36\ \mu m$, $t = 15'$, $V = 30$ V; *b*, $t = 30'$, $V = 30$ V; *c*, $t = 30'$, $V = 60$ V. Other parameters as in Fig. 3.

cannot be neglected without losing information on this transition.

V. Backdiffusion Results

It has been well known for some time that backdiffusion with the original ion that was present in the glass can be used to bury the profile under the surface of the substrate. This has two advantages: the profile is more symmetrical without the large discontinuous index jump at the glass–cover interface (this improves the coupling to optical fibers), and the optical energy propagates away from surface irregularities that may cause unwanted scattering. Such backdiffusion is carried out without mask at the surface, and in this case the next flux of ions is one dimensional along the depth direction only. The driving field is simply given by $E_x = V/d$ and $E_y = 0$. A typical example is shown in Fig. 5, starting from a profile exchanged in conditions such that the resulting depth-to-width ratio is maximized, i.e., mask opening much smaller than exchange depth. We see how the maximum of the profile moves quite far under the surface. However, the result is still far from symmetrical because the index gradient is much larger on the substrate side than on the cover side. The field seems to push the maximum of the profile against its tail end. Furthermore, the profile is still quite elliptical. The same behavior shows up in measured backdiffused profiles given in Ref. 2. It may be of interest to note that the result of Fig. 5(c) was recalculated with $V = 90$ V and $t = 30$ min instead of $V = 30$ V and $t = 90$ min with identical results (within 1–2% due to the small difference in the thermal contribution). Again this result is in the regime where the external field driving is dominant.

VI. Annealing Results

To improve on the symmetry and ellipticity of the profile, annealing a backdiffused waveguide was carried out. Since annealing is performed in the absence

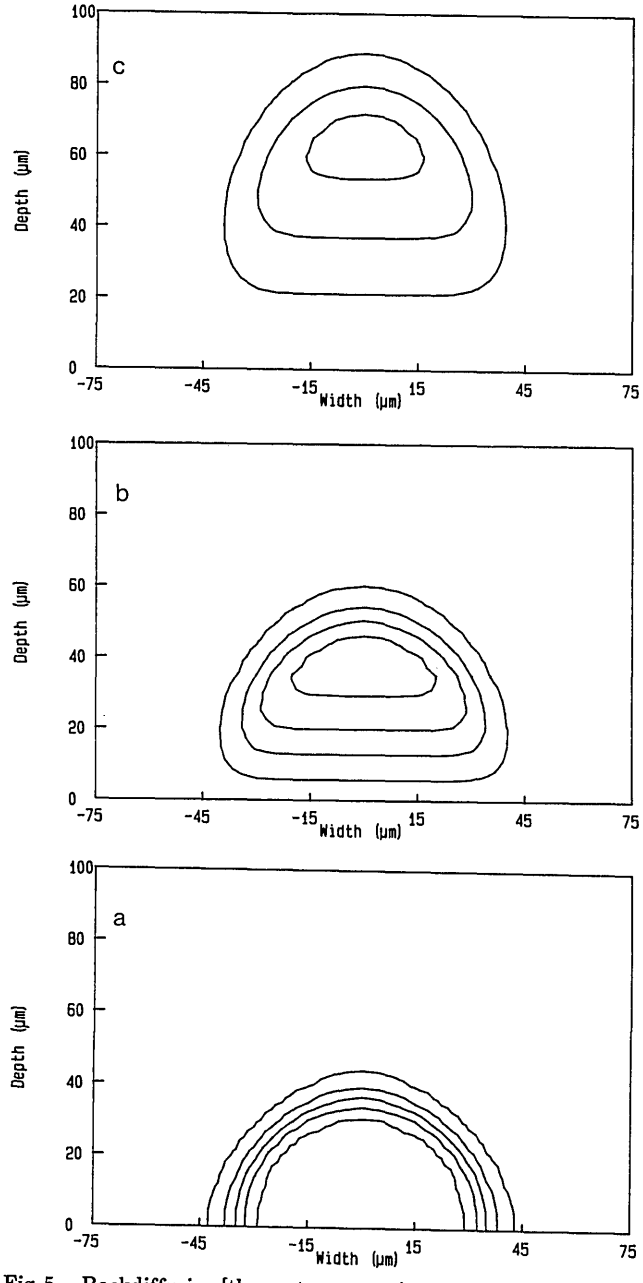

Fig. 5. Backdiffusion [the contours remain normalized to the maximum of the original profile 5(a)]: (a) original exchange: $D = 4\ \mu m$, $\alpha = 0.5$, $t = 30'$, $V = 30$ V; (b) backdiffusion (no mask), $t = 30'$, $V = 30$ V; (c) additional backdiffusion, cumulative $t = 90'$, $V = 30$ V.

of sources or sinks for the ions, no external field may be used because there cannot be a net flux in the glass.

From Eq. (16), we see that the driving force for the concentration change in the absence of external fields is made up of two contributions. The first term leads to a concentration increase where the profile is concave (positive curvature $\nabla^2 c$) and a decrease where it is convex. The second term is always positive and strongest where the gradient is largest. Therefore, apart from the intuitively obvious conclusion that annealing reduces the index near the maximum and increases it near the edges of the profile (making the profile larger

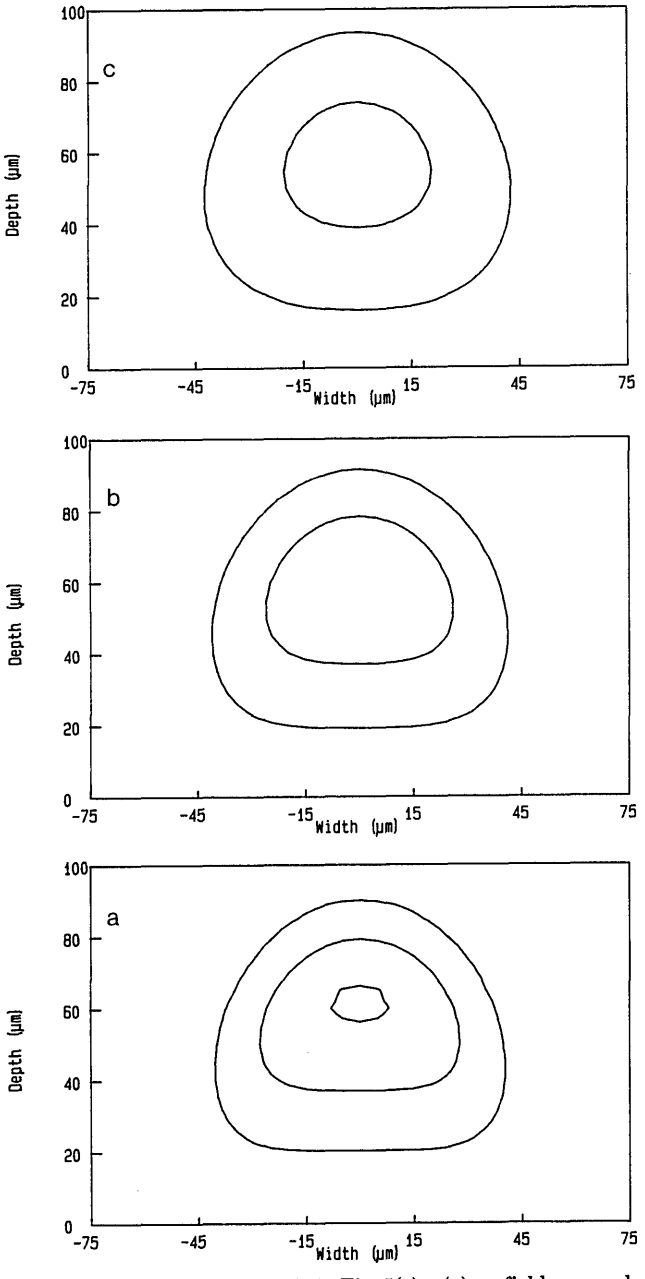

Fig. 6. Annealing of the profile in Fig. 5(c): (a) no field, no mask, no sources, $t = 120'$; (b) cumulative $t = 240'$; (c) cumulative $t = 600'$.

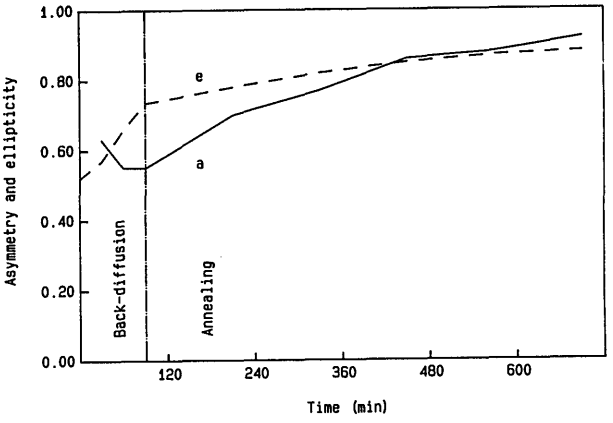

Fig. 7. Ellipticity e and asymmetry a of the profiles shown in Figs. 5 and 6 (parameters defined in the text).

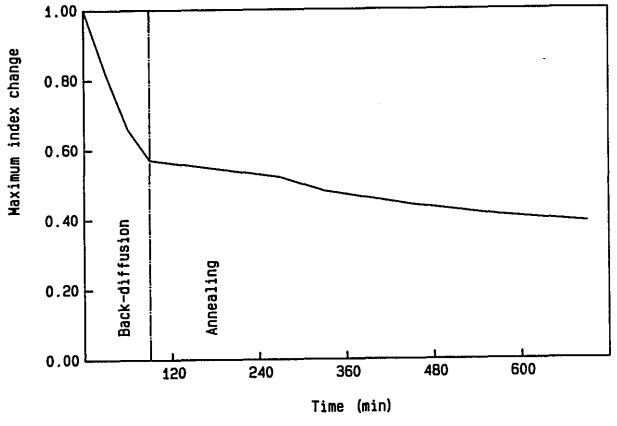

Fig. 8. Maximum index change of the profiles shown in Figs. 5 and 6 [normalized to the maximum occurring in Fig. 5(a)].

in size but with lower maximum concentration values), we see that this effect occurs faster in the stronger gradient regions. This should decrease the difference in the magnitude of the gradients on either side of the maximum in the depth direction and lead to more symmetric index profiles.

To verify this point, the last profile in the sequence of backdiffusion [Fig. 5(c)] was annealed for 10 h in increments of 1.5 h. Some results are shown in Fig. 6. We see that the profile does become more symmetrical and less elliptical. To quantify these observations, the ellipticity e was calculated on all the profiles starting from the original one [Fig. 5(a)] as the ratio of the sizes of the 0.5 contour line in the depth and lateral directions, respectively. The asymmetry a was also calculated as the ratio of the distance between the maximum of the profile and the 0.3 contour line toward the substrate and the cover, respectively. In these calculations, the contour lines used were those of renormalized profiles relative to the maximum concentration for each case so that the sizes measured were representative of the whole profile.

The result of these calculations is shown in Fig. 7 with backdiffusion occurring for the first 90 min and annealing for the rest of the time. The ideal situation of a symmetrical circular profile occurs when $a = e = 1$. We see that backdiffusion decreases the ellipticity but worsens the asymmetry (because of the already noted effect of gradient tightening on the substrate side of the maximum). In the annealing stage, however, both ellipticity and asymmetry are improved and the profile tends to become more fiberlike. This confirms the predicted properties of annealing in diminishing the gradient nonuniformities.

In addition to the size and shape of the index profile, a parameter of interest in the field matching of fibers to channel waveguides is the magnitude of the index change. Figure 8 shows the evolution of this quantity relative to its value for the initial guide of the sequence.

Since backdiffusion actually removes dopant ions from the glass, while annealing only redistributes them, the decrease is much more pronounced in the former case. The starting value of index change is determined by the process used: near 0.09 for Ag^+–Na^+ exchange and 0.009 for K^+–Na^+ exchange in a soda-lime glass, for example.

VII. Conclusion

We have developed and solved a model for 2-D field-assisted ion exchange in glass that, we believe for the first time, takes into account most factors affecting the diffusion of the ions. Space charge effects are partially included in the sense that the total electric field inside the substrate has nonzero divergence. The other phenomena that remain to be included are the mixed alkali effect[13] (reduction of individual alkali ion mobility when another type of alkali ion is present) and the charge depletion that is believed to occur under the masked areas.[12]

This model provides a more realistic modeling of the profile from the fabrication conditions and will enable optical circuit designers to have better control over the performance of their devices.[14] The effects of backdiffusion and annealing are calculated and discussed in the context of decreasing the mismatch between standard graded index multimode fibers and channel guides. A particular example shows how to achieve almost perfect circular symmetry in a buried channel guide by a proper sequence of backdiffusion and annealing. Although the results presented are limited to large multimode channel waveguides, the conclusions of this work apply equally well to smaller single-mode guides. In fact, it was shown in Sec. II that the calculations are invariant under a global scale change as long as the voltages and durations are adjusted accordingly. Therefore, the scale of all the figures presented could be reduced to represent single-mode guides, but the fabrication parameters given in the captions would have to be changed.

Parts of this paper were presented at the 1989 SPIE Symposium on Optoelectronic and Fiber Optic Devices and Applications.

References

1. R. V. Ramaswamy and R. Srivastava, "Ion-Exchanged Glass Waveguides: A Review," IEEE/OSA J. Lightwave Technol. **LT-6,** 984–1002 (1988).
2. H. J. Lilienhof, E. Voges, D. Ritter, and B. Pantschew, "Field-Induced Index Profiles of Multimode Ion-Exchanged Strip Waveguides," IEEE J. Quantum Electron. **QE-18,** 1877–1883 (1982).
3. A. Tervonen, S. Honkanen, and M. Leppihalme, "Control of Ion-Exchanged Waveguide Profiles with Ag Thin-Film Sources," J. Appl. Phys. **62,** 759–763 (1987).
4. C. Nissim, A. Beguin, R. Jansen, and P. Laborde, "Fabrication and Characterization of Buried Single-Mode Waveguides and Couplers made by Ion Exchange in Glass," in *Technical Digest, Optical Fiber Communication Conference* (Optical Society of America, Washington, DC, 1989), paper WM2.
5. R. H. Doremus, "Ion Exchange in Glasses," in *Ion-Exchange, Vol. 2,* J. A. Marinsky, Ed. (Marcal Dekker, New York, 1969).
6. S. D. Fantone, "Refractive Index and Spectral Models for Gradient-Index Materials," Appl. Opt. **22,** 432–440 (1983).
7. R. G. Walker, C. D. W. Wilkinson, and J. A. H. Wilkinson, "Integrated Optical Waveguiding Structures Made by Ion-Exchange in Glass. 1: The Propagation Characteristics of Stripe Ion-Exchanged Waveguides; a Theoretical and Experimental Investigation," Appl. Opt. **22,** 1923–1928 (1983).
8. M. Abou-El-Leil and A. R. Cooper, "Analysis of Field-Assisted Binary Ion-Exchange," J. Am. Ceram. Soc. **62,** 390–395 (1979).
9. S. N. Houde-Walter and D. T. Moore, "Gradient-Index Profile Control by Field-Assisted Ion Exchange in Glass," Appl. Opt. **24,** 4326–4333 (1985).
10. E. Voges, "Planar Tees and Star Couplers," in *Integrated Optics,* S. Martellucci and A. N. Chester, Eds. (Plenum, New York, 1983). Note that the expression for the electric field cited here is corrected from that of Ref. 2 with a square root on the right-hand side.
11. H. Yoshida and T. Kataoka, "Migration of Two Ions During Electrolysis of Glass Waveguide," J. Appl. Phys. **58,** 1739–1743 (1985).
12. S. Honkanen, Nokia Research Center Espoo, Finland; private communication.
13. R. H. Doremus, "Mixed-Alkali Effect and Interdiffusion of Na and K Ions in Glass," J. Am. Ceram. Soc. **57,** 478–480 (1974).
14. A. Beguin, T. Dumas, M. J. Hackert, R. Jansen, and C. Nissim, "Fabrication and Performance of Low Loss Optical Components Made by Ion Exchange in Glass," IEEE/OSA J. Lightwave Technol. **LT-6,** 1483–1487 (1988).